DOI: 10.4408/IJEGE.2014-01.O-03

DETECTION OF PAST SLOPE ACTIVITY IN A DESERT AREA USING MULTI-TEMPORAL DINSAR WITH ALOS PALSAR DATA

Alfredo ROCCA[(*,**)], Paolo MAZZANTI[(*,**)], Daniele PERISSIN[(***)] & Francesca BOZZANO[(*,**)]

[(*)] *Sapienza University of Rome - Department of Earth Sciences - P.le Aldo Moro, 5 - 00185 Rome, Italy*
[(**)] *NHAZCA s.r.l. - Spin-off Sapienza Università di Roma - Via Cori, snc - 00177 Rome, Italy*
[(***)] *Purdue University - Lyles School of Civil Engineering - 550 Stadium Mall Drive, West Lafayette, IN 47907, USA*

EXTENDED ABSTRACT

Il presente lavoro illustra i risultati di uno studio di un versante costiero nel Sultanato dell'Oman (penisola Arabica) che, tra il 2011 e il 2012, ha subito alcuni processi d'instabilità gravitativa in corrispondenza di aree interessate dalla costruzione di una strada tra Hasik e Ash Shuwaymiyyah (Governatorato di Dhofar). Un'analisi condotta tramite interferometria SAR (Synthetic Aperture Radar) satellitare, ha consentito di caratterizzare la dinamica evolutiva di tale versante identificando i fenomeni più significativi di attività da un punto di vista temporale e spaziale.

L'area di studio, localizzata nella regione di Dhofar, si trova all'interno del graben di Hasik, a nord della foce del Wadi Dahanat. La zona è caratterizzata dalla deformazione Oligocenica del margine passivo relativo all'apertura del rift di Aden. Sovrapposte al basamento proterozoico (~800 Ma; Mercolli *et alii*, 2006) si rinvengono nell'area diverse unità calcaree, appartenenti alla serie Eocenica del gruppo di Hadramaut, tipiche di una deposizione marina di acque poco profonde. Dopo la deformazione Oligocenica, una nuova fase tettonica all'inizio del Miocene ha coinvolto le unità sedimentarie definendo una linea costiera con scogliere disposte a diverse quote. In tale contesto è localizzato il versante costiero oggetto di studio, ai piedi di una parete sub-verticale, laddove si riconosce la presenza di una spessa coltre detritica con blocchi di decine di metri cubi e con evidenze di passati processi di instabilità gravitativa (Platel & Roger, 1989; Roger *et alii*, 1989; Bechennec *et alii*, 1993; Watchorn *et alii*, 1998, Robertson & Bamkhalif, 2001, Ghezzi *et alii*, 2012).

Le analisi SAR Interferometriche satellitari (DInSAR) (Massonnet *et alii*, 1993; Hanssen, 2001; Strozzi *et alii*, 2005, 2010; Jebur *et alii*, 2013) sono state applicate al fine di acquisire informazioni quantitative sui processi deformativi avvenuti negli ultimi anni, Le tecniche DInSAR, infatti, soprattutto nella loro declinazione avanzata "A-DInSAR" (Advanced DInSAR), consentono, di sfruttare le immagini acquisite nel tempo dai satelliti su una stessa area per estrarre informazioni sull'evoluzione dei processi deformativi con elevata accuratezza (Ferretti *et alii*, 2001, 2011; Berardino *et alii*, 2002; Perissin & Wang, 2012). Le tecniche A-DInSAR, tuttavia, richiedono la disponibilità di numerose immagini per ottenere informazioni di spostamento affidabili e con accuratezze elevate. L'area oggetto del presente studio risulta tuttavia coperta da poche immagini d'archivio dei satelliti dell'Agenzia Spaziale Europea, insufficienti per l'applicazione di metodologie A-DInSAR. Un numero maggiore di immagini è stato invece acquisito dal satellite ALOS PALSAR (Advanced Land Observation Satellite - Phased Array type L-band Synthetic Aperture Radar), gestito dall'Agenzia Spaziale Giapponese JAXA (Japanese Aerospace Exploration Agency). Le nove immagini acquisite da ALOS PALSAR tra il dicembre 2006 e l'aprile 2010, benché insufficienti per eseguire analisi A-DInSAR, si sono rivelate utili per osservare la presenza di spostamenti sul versante indagato attraverso l'analisi manuale condotta sugli interferogrammi calcolati. Più in dettaglio, sono stati generati interferogrammi ridondanti (ciascuna immagine è stata accoppiata con tutte le altre) e i più coerenti sono stati utilizzati per analizzare il segnale di fase interferometrica, con l'obiettivo di stimare gli spostamenti filtrando il segnale dai contributi di fase dovuti alla topografia (quota). Tale risultato è stato ottenuto analizzando, per ciascun interferogramma, i parametri relativi alla distribuzione temporale delle immagini e alla cosiddetta baseline normale (proporzionale alla distanza tra i satelliti durante l'acquisizione delle immagini), che è direttamente correlabile con la sensibilità del sistema di osservare e quantificare il dato relativo alla quota altimetrica.

Attraverso questa metodologia è stato possibile riconoscere sul versante tre aree circoscritte che hanno subito degli spostamenti nell'intervallo di tempo compreso tra giugno 2008 e giugno 2009.

Il metodo di analisi DInSAR utilizzato in questo lavoro ha consentito di estrarre informazioni sui processi deformativi nonostante le poche immagini disponibili. A tal proposito, è bene osservare che l'applicazione di algoritmi automatici per la stima degli spostamenti avrebbe potuto ridurre l'osservabilità di tali processi a causa della discontinuità spaziale e temporale degli spostamenti stessi.

Tale approccio può essere considerato quindi una soluzione investigativa utile in aree remote e non urbanizzate, dove è disponibile una limitata conoscenza sulle condizioni geomorfologiche e geologiche locali e laddove non esistono altri dati di monitoraggio sull'evoluzione storica dei fenomeni deformativi.

ABSTRACT

Coastal slope involved in the construction of a road in the Sultanate of Oman was affected during the period 2011-2012 by instability processes. Lithological and geomorphological evidence suggested a general conformation of the slope that is very prone to gravitational instability processes. Because satellite SAR interferometry (InSAR) is the only technique that is able to provide quantitative information about past ground displacements, it has been chosen to investigate the past evolution of the slope. Nine archived SAR images acquired by the ALOS PALSAR have been analysed using a hybrid approach based on the classical differential interferometry (DInSAR) and Quasi-Persistent Scatterers (QPS) techniques. Some ground deformation processes have been detected and measured on three portions of the slope. One of them has been localised within the area affected by the recent landslide phenomenon. Thanks to this approach the deformation processes have been defined in time and the related displacements have been quantitatively estimated.

Key words: *Oman, landslides, SAR interferometry, DInSAR, A-DInSAR, ALOS PALSAR*

INTRODUCTION

The use of Earth Observation (EO) data for the investigation of remote areas (deserts, forests and generally areas with insufficient lines of communication) plays a key role in acquiring both preliminary information and monitoring data for several fields of infrastructure and natural hazard management (Barrett, 2013). Among spaceborne EO techniques, Synthetic Aperture Radar (SAR) represents an interesting and widely used tool. Because SAR systems are based on active sensors, they are able to provide information both night and day and in the presence of cloud coverage, thus expanding upon the opportunities offered by optical systems. Characteristic of radar sensors is the use of coherent signals, i.e., the capability of retaining information about the phase component of the electromagnetic signal. Therefore, the pixels of the SAR images include both amplitude and phase terms. The former is related to the reflection intensity of the scattering targets, and the latter is related to sensor-target distance. This peculiarity has been exploited in recent decades, turning earth observation spaceborne SAR systems into tools to provide quantitative data, using interferometric processing techniques (InSAR).

Multi-pass classical InSAR is performed by coupling SAR images to generate a single interferogram to perform phase signal analyses (Li & Goldstein, 1987; 1990; Gabriel & Goldstein, 1988; Goldstein *et alii*, 1988; Prati *et alii*, 1990; Hanssen, 2001; Simons *et alii*, 2002; Tong *et alii*, 2010). The phase signal of a single interferogram, however, carries information related to several contributions (e.g., topography, displacement, atmospheric artefacts, and noise). If the temporal baseline (namely, the time interval between the acquisition of the two repeat pass scenes used to compute the interferogram) is short enough, we can assume that no displacement occurred and thus ascribe all phase signals to topographic contribution. In contrast, to acquire information about displacements that occurred in the time interval between the acquisitions of two SAR scenes, the topographic contribution can be subtracted from the derived interferogram (e.g., by an available Digital Elevation Model). In the latter case, this technique, known as Differential InSAR - DInSAR, has been successfully applied in the investigation of various ground deformation processes. DInSAR provides good results for the investigation of displacement characterised by wide, spatially smooth deformation processes, such as coseismic and postseismic deformations (Massonnet *et alii,* 1993; 1994), volcanic deformation processes (Massonnet *et alii,* 1995) or ice and glacier dynamics (Goldstein *et alii,* 1993; Kwok & Fahnestock, 1996). However, landslide displacements have also been detected and measured by DInSAR (Carnec *et alii*, 1996; Fruneau *et alii*, 1996; Singhroy *et alii*, 1998; Singh *et alii*, 2005; Strozzi *et alii*, 2005; 2010; Riedel & Walther, 2008; García-Davalillo *et alii,* 2014; Jebur *et alii,* 2013).

As stated above, one of the primary limitations of DInSAR is the difficulty in separating the different contributions affecting the interferometric phase signal. Moreover, DInSAR cannot be supported by effective solutions for the detection and removal of an atmospheric disturbance. Finally, noise caused by temporal decorrelation (i.e., a long time interval between multi-pass SAR scene acquisition) and/or geometrical decorrelation (i.e., long distance between positions occupied by satellite during scene acquisition) can seriously prevent the attainment of useful interferometric results.

To compensate for these limitations, several data processing approaches have been proposed, namely Advanced DInSAR (A-DInSAR). All of them exploit long time series of SAR images of the same area to attain some common results: i) estimation and removal of atmosphere artefacts (i.e., Atmosphere Phase Screen - APS); ii) contemporary estimation of several phase contributions (at least, topography and displacement); iii) capability of providing time series of deformation along the whole time interval. The development and diffusion of Advanced Differential SAR Interferometry (A-DInSAR) methods over the last decade have significantly increased the range of applications of SAR data for past-oriented investigation and for future monitoring of ground displacements (Ferretti *et alii,* 2001; 2011; Berardino *et alii,* 2002; Hooper *et alii*, 2004; Lanari *et alii*, 2004; Lauknes, 2004; Kampes, 2006; Van Leijen & Hanssen, 2007; Perissin, 2008; Stramondo *et alii*, 2008; Perissin *et alii*, 2011; 2012; Bozzano & Rocca, 2012).

From this perspective, if DInSAR is able to provide a "snapshot" of a given deformation process in the time interval between the acquisition of two scenes, A-DInSAR approach is actually able to provide displacement information over time, such as long-term time series of displacement.

However, some conditions need to be satisfied to perform A-DInSAR analysis, such as the availability of a large quantity of SAR images (conventionally, greater than 20) acquired with the same geometric and radiometric features over the same area. However, especially in remote areas, this condition cannot be always satisfied by space agency archives.

For the area investigated in this chapter, only few archive images from the ALOS PALSAR, ERS and Envisat sensors were available; hence, DInSAR analyses were performed using a redundant approach suitable for increasing the reliability of the attained results.

The study presented herein is of a coastal slope in the Dhofar region in the Sultanate of Oman involved in the construction of a major road (Hasik - Ash Shwaimiyah Project). As the slopes experienced some gravitational instability processes during construction activities during the period August 2011-June 2012, our objective was to better understand the stability conditions of such a slope before the above-mentioned time interval. To attain quantitative information related to past displacements, InSAR based approaches represent the only available solutions.

STUDY AREA

The study area is in the Dhofar region (Oman, in the eastern Arabian Peninsula) (Fig. 1), located inside the Hasik graben, north of the riverbed of Wadi Dahanat (almost always dry). The area under investigation is a steep barren slope under a high cliff facing the Kuria Muria Bay. The slope, affected by instability issues, has been involved in the construction of a road to connect Hasik to the northern village of Ash Shuwaymiyyah.

GEOLOGICAL AND GEOMORPHOLOGICAL SETTING

The Hasik Graben is an Oligocene onshore deformation zone of the passive margin related to the oblique opening of the oceanic basin of the Aden Rift. The Hasik Graben (10 km wide and 30 km long) is bounded to the North and South by two master normal faults with a N45°E to N75°E trend and presents an axial dip towards the east (Fig. 2) (Fournier *et alii*, 2004).

Several paleo-environments have characterised the deposition during the Tertiary period. Transgressive cycles with the deposition of shallow marine formations and regressive cycles evidenced by the deposition of gypsum began in the Late Palaeocene (60 Ma) and ended in the Late Eocene (38 Ma) (Roger *et alii*, 1989; Watchorn *et alii*, 1998).

A carbonate succession up to 1000 m thick is exposed, characterised by three sedimentary groups (Platel & Roger, 1989; Roger *et alii*, 1989; Bechennec *et alii*, 1993; Robertson & Bamkhalif, 2001), which correspond to pre-rift, syn-rift and post-rift stages of deposition, the Hadhramaut, Dhofar and Fars groups, respectively. The study area is dominated by the Eocene series of the Hadhramaut group, whereas the Dhofar group (syn-rift) locally outcrops in the northern part of this sector. The post-rift Fars group, instead, does not outcrop in the study area and is restricted to the Salalah plain (Fig. 2).

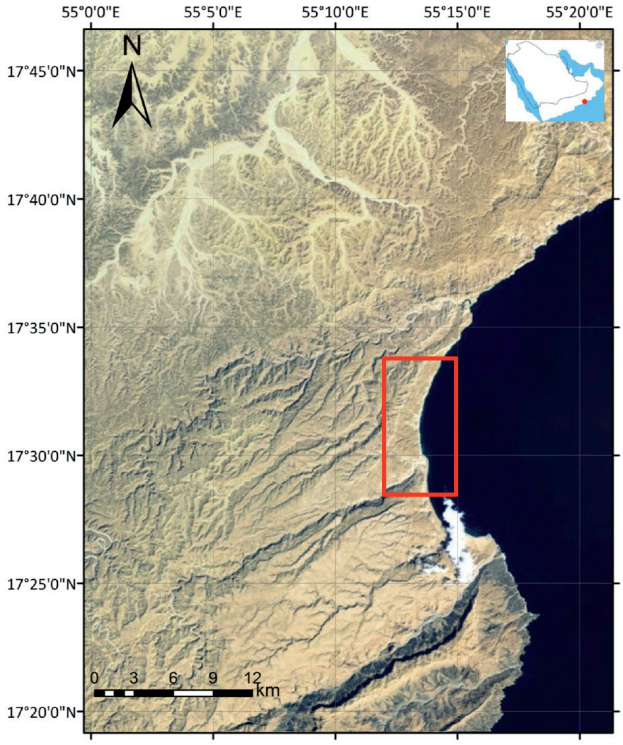

Fig. 1 - Geographic location of the study area

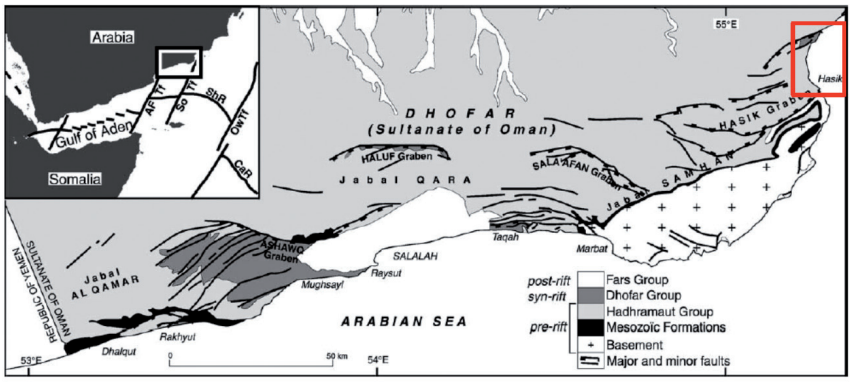

Fig. 2 - Structural map and sedimentary units of Southern Dhofar, Sultanate of Oman, derived and simplified from the 1/250,000 geological maps of Salalah and Hawf (Platel et alii, 1992; Roger et alii, 1992); in addition, the main structures of the Gulf of Aden and the on-land study area are present. Abbreviations are as follows: AF Tf: Alula-Fartak Transform Fault; So Tr: Socotra Transform Fault; Ow Tr: Owen Transform Fault; ShR: Sheba Ridge; CaR: Carslsberg Ridge. The red box identifies the study area (from Lepvrier et alii, 2002, mod.)

Focusing on the study area (Fig. 3), the Hadhramaut group, which in turn overlies the Proterozoic basement (~800 Ma; Mercolli *et alii*, 2006), consists of carbonate units typical of shallow-water conditions, including the massive limestone of the Umm Er Radhuma Formation and the Rus Formations (up to 600 m thick, late Palaeocene/Thanetian - early Eocene/Ypresian), the Dammam formation (middle Eocene/Lutetian-Bartonian), consisting of yellow shale and chalky marl with interbedded argillaceous limestone (thickness 43 meters) and fine to medium grained creamy limestone, sometimes marly and chalky, nodular or dolomised (thickness approximately of 200 meters), and finally the Aydim formation (late Eocene/Priabonian), consisting of limestone, chalky marl and calcarenitic deposits characterised by rich macrofauna and banks of corals.

The syn-rift Dhofar group, unconformably deposited on the Hadhramaut group, consists of lacustrine limestone at the base (100 m), overlain by platform limestone (Ashawq Formation, 600 m), which passes laterally at the top to the overlying, chalky calci-turbidic deposits of the late Oligocene to early Miocene Mughsayl Formation (700 m thick beneath the Salalah plain; Platel *et alii*, 1992). The slope deposits of the Mughsayl Formation, which include megabreccia, debris flows, and olistolitic material transported from the adjoining shelf, result from the collapse and subsidence of the margin and correspond to deeper depositional environments.

After the Oligocene tectonic phase, a tectonic readjustment occurred in the Early Miocene so that the sedimentary package extended to the sea of the Kuria Muria Bay with a coastline of cliffs at different elevations, defined ridges tilting to the North-West, stacked as tumbled dominos one on top of another, creating overhangs and ledges (Ghezzi *et alii*, 2012).

At the end of the Early Miocene, the sedimentary conditions become similar to the present, in accordance with the general emersion of the South Arabian plate in that period. Thus, subsequent retrogressive-transgressive marine cycles of the Middle Miocene and the youngest of the Pliocene and Pleistocene combined with a possible late tectonic can be responsible for erosional and depositional phenomena involving the tertiary formations.

Finally, not depicted on the map in Fig. 3 for scale reasons, two quaternary terms outcrop, related to colluvial and alluvial deposits. The quaternary colluvium is particularly interesting for the objective of the present work because it is located on the coastal slope under investigation. It is composed of rock debris accumulated at the foot of the cliffs caused by landslides below the fault scarps and consists of limestone blocks of up to 30 cubic meters in average size with marl and gypsum inside a silt matrix, extending towards the sea. The thickness is several tens of meters (more

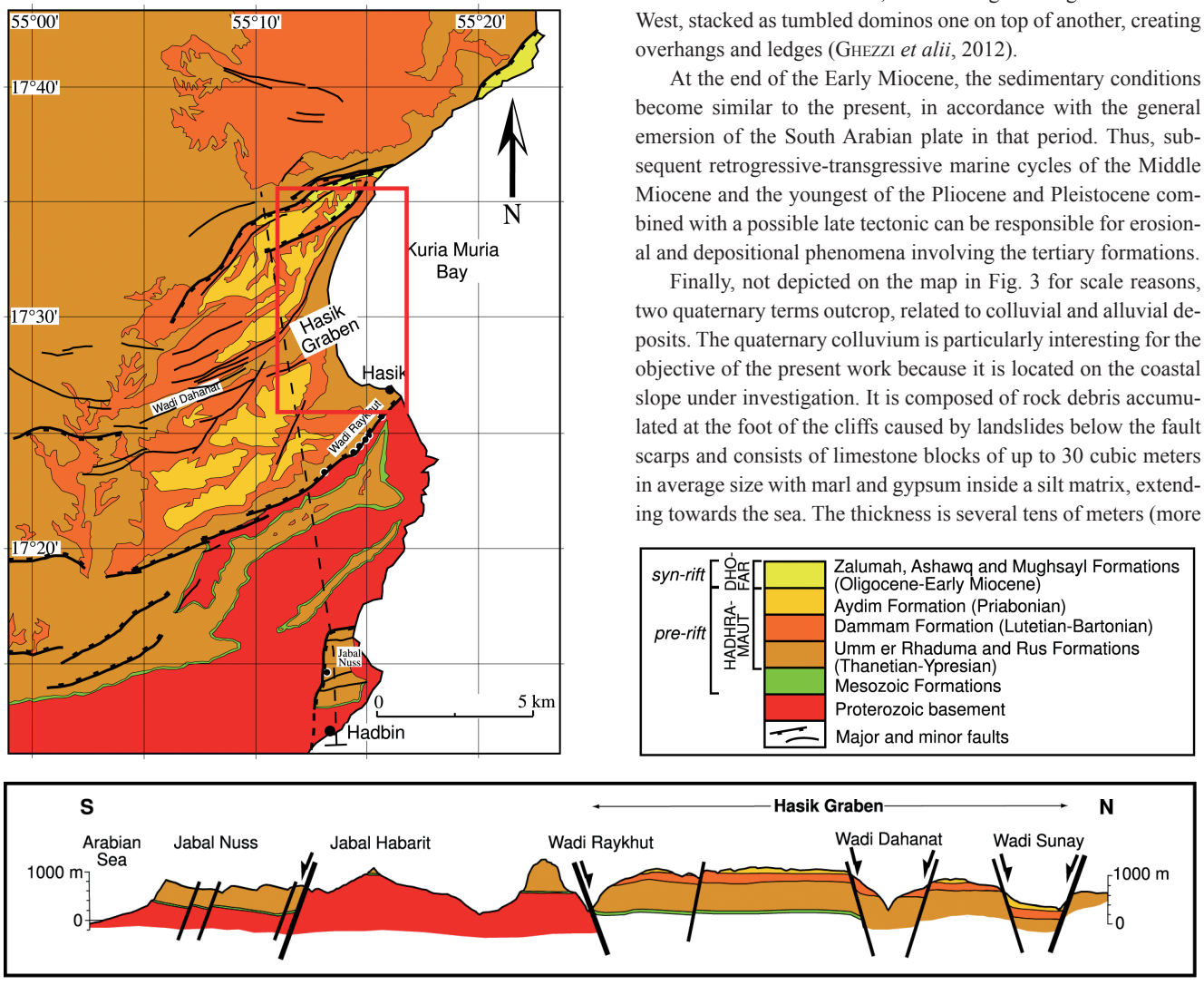

Fig. 3 - Geological map of the "Hasik Graben" area. The red box identifies the study area (from Fournier et alii, 2004; modified)

than 20 meters). The screes formation is still on-going from the Pleistocene. To conclude, there are also very thin (20-50 cm) alluvial deposits on the Wadi Dahanat floor consisting primarily of boulders emplaced during the last pluvial phase at the end of Pleistocene (Ghezzi *et alii*, 2012).

From the geomorphological perspective, the slope, which is primarily involved through the presence of the above-mentioned colluvial deposit, presents evidences of phenomena of past gravitational instability. According to Ghezzi *et alii* (2012), these geomorphologic features seem linked to the following causes: i) different phases of the sea level in different eras caused some terraced planes located at different elevations. Consequently, the movement of the collapsed deposits increased, generating new collapses; and ii) the strong supply of sediments eroded by the Wadi Dahanat and its minor tributary are transported to the sea over time.

These characteristics are located particularly in the southern half of the study area, north of the mouth of the Wadi Dahanat. In the northern part of the sector under investigation, evidence of past instability processes involving the quaternary colluvium seem less severe; this can most likely be related to the decreased thickness of the colluvium layers (Ghezzi *et alii*, 2012).

During the period August 2011-June 2012, slope instability processes affected the area involved in the construction of the Hasik - Ash Shwaimiyah road. Because we were interested in the spatial and temporal evolution of the slope dynamics before the beginning of the construction, past information needed to be acquired about the slope under investigation. To reach this aim, InSAR-based techniques have been selected as the most effective for the presented purpose because they are the only techniques able to provide quantitative information on past ground displacements

.

MULTI-TEMPORAL DINSAR ANALYSES

C-BAND ARCHIVE SAR IMAGES

The SAR data archives contain very few images related to the study area. In particular, only four multi-temporal images acquired by the ERS-1 and ERS-2 satellites (European Space Agency - ESA) between 1992 and 1996 were available in the ESA archive (Tab. 1). More recent data have been acquired by ESA using the Envisat satellite; however, the best interferometric stack reached only five scenes for the 2003-2004 period (Tab. 2).

L-BAND ARCHIVE SAR IMAGES

More archival images have been acquired by the ALOS satellite (Advanced Land Observation Satellite) using the PALSAR sensor (Phased Array type L-band Synthetic Aperture Radar) and archived by JAXA (Japanese Aerospace Exploration Agency).

Nine images, acquired in the period between the end of 2006 and the middle of 2010, were available. We used 4 Fine Beam Single Polarisation (FBS, bandwidth: 28 MHz) images and 5

	Acquisition date (yyyymmdd)	Satellite	Band (wavelength)	Orbital Geometry	Track
1	19920529	ERS-1	C (5.66 cm)	Descending	392
2	19930305	ERS-1			
3	19960422	ERS-2			
4	19960527	ERS-2			

Tab. 1 - Available dataset acquired by ERS satellites

	Acquisition date (yyyymmdd)	Satellite	Band (wavelength)	Orbital Geometry	Track
1	20030908	Envisat	C (5.62 cm)	Descending	392
2	20031013				
3	20031117				
4	20040510				
5	20040614				

Tab. 2 - Available dataset acquired by Envisat satellite (ASAR sensor)

	Acquisition date (yyyymmdd)	Satellite	Band (wavelength)	Orbital Geometry	Track
1	20061223	ALOS	L (23.6 cm)	Ascending	570
2	20070810				
3	20071226				
4	20080512				
5	20080627				
6	20090630				
7	20090815				
8	20091231				
9	20100402				

Tab. 3 - Available dataset acquired by ALOS satellite (PALSAR sensor)

Fine Beam Double polarisation (FBD, bandwidth: 14 MHz) images. The pixel spacing of the fine beam single polarisation (FBS) data is 4.68 m in the range direction and 3.17 m in the azimuth direction, whereas the pixel spacing of the double polarisation (FBD) images is 9.36 m in the range direction by 3.17 m in the azimuth direction (Chen *et alii*, 2012) (Tab. 3). Using the same central frequency, the range bands of the FBS and FBD images are fully overlapped. This allowed interferometric processing to be performed, combining FBS and FBD images in the same interferometric pair using the common HH polarisation [for this objective, the FBD data needed to be doubly oversampled in range to ensure the same resolution for all images used in the dataset (Chen *et alii*, 2014)].

The primary difference between the data from the ESA satellites and those acquired by the ALOS PALSAR is represented by the different wavelengths. L-band SAR images from ALOS are characterised by much longer wavelengths (more than 23 cm), four times longer than the C-band data. Using longer wavelengths, the interferograms generated are characterised by higher spatial coherence. Decorrelation is much less severe for temporal, geometrical and atmospheric effects. The so-called "critical baseline" (namely, the value of the Bn above which an interferogram

	ERS – Envisat	ALOS PALSAR
Wavelength	~ 56 mm	~ 236 mm
Altitude	790 km	700 km
Look angle*	23 degrees	34.3 degrees
Bandwidth	15.55 MHz	FBS: 28 MHz; FBD: 14 MHz
Critical Baseline	1.1 km	FBS: 13 km; FBD: 6.5 km

*Other look angles are available for ALOS, but 34.3 degrees is the main one

Tab. 4 - Comparison between ERS/Envisat and ALOS PALSAR data (from Wei & Sandwell, 2010 mod.)

is totally decorrelated) is much higher (several kilometres) (Tab. 4). For this reason, a given data-stack whose normal baselines of image pairs are usually largely below this threshold can be fully exploited to obtain useful information.

The critical baseline is given by:

$$B_c = \frac{\lambda R \tan\theta}{2\Delta\rho}$$

where B_c is the critical baseline, λ is the sensor wavelength, R is the slant range distance from the satellite to the reflector on the Earth surface, θ is the incidence angle, and $\Delta\rho$ is the radar range resolution.

Moreover, the same consideration can be applied to the risk of losing information from SAR images acquired with long temporal baselines. Comparing C-band and L-band data, the latter appear considerably resilient to temporal decorrelation effects over the same areas, as quantitatively demonstrated by Wei & Sandwell (2010). Finally, it is notable that the available images belong to an ascending geometry stack and are thus able to provide more appropriate LOS orientation along the observed slope compared with that achievable by descending ERS and Envisat stacks, as illustrated below.

ANALYSES OF ARCHIVED SAR DATA

Regarding C-band images, with such a poor data stack, only a few differential interferograms could be computed, even assuming complete connection between the images to generate maximum redundancy of interferograms (images are connected to one another). In this case, considering N(N - 1)/2 interferograms to have a complete connection (where N is image number), we had only six and ten interferograms for the ERS and Envisat stacks, respectively (Fig. 4). Moreover, most of the computed interferograms were characterised by long normal baselines (Bn), which negatively influence the spatial coherence.

Most of the generated interferograms were extremely noisy, primarily because of geometrical decorrelation effects. For this reason, only one ERS and four Envisat interferograms were characterised by an acceptable coherence for the analysis of past displacements. Considering such conditions and the small quantity of available data, the application of A-DInSAR methods was not feasible. Moreover, the analysis of differential interferograms characterised by higher spatial coherence was insufficient to detect and measure the presence of displacements during the period of investigation.

Furthermore, both the ERS and Envisat datasets were acquired along descending orbital paths so that the LOS was characterised by a stronger component perpendicular to the slope under investigation (i.e., the worst condition under which to observe possible displacements along the slope direction) (Fig. 5).

With the L-band SAR signal (23.6 cm wavelength) and the greater number of available images, the interferometric results were significantly better than those attained from the C-band data processing (ERS and Envisat). However, even the ALOS PALSAR stack with its potentially high coherent interferograms contains few images, insufficient to perform reliable A-DInSAR

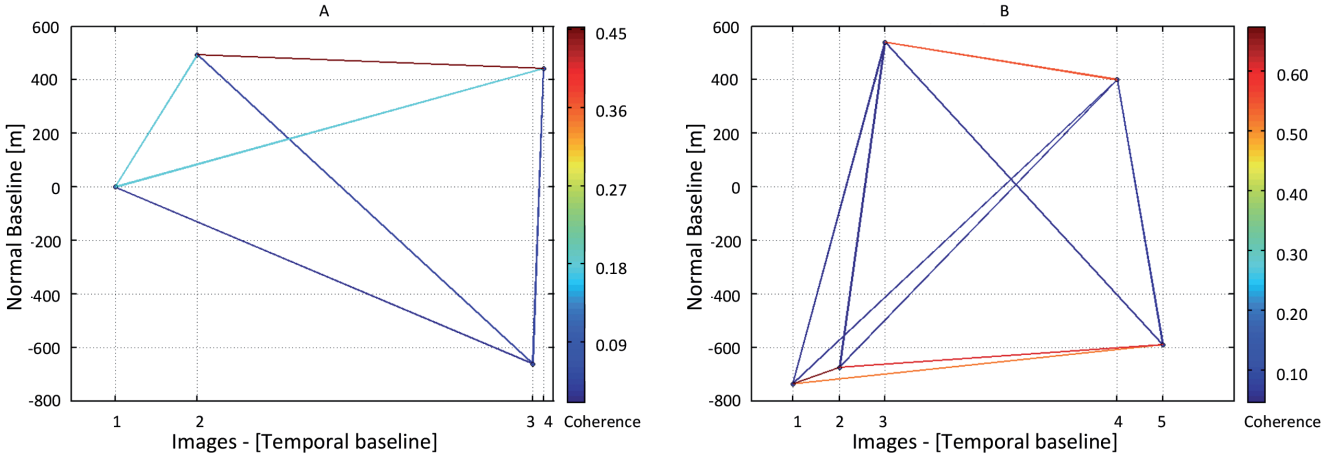

Fig. 4 - Graphs showing images connections related to ERS (A) and Envisat (B) data-stacks. Each dot represents an image in accordance with numeration of Tab. 3.1 and Tab. 3.2. Images are plotted in time (X axis) and space, represented by normal baseline (Y axis). Each line represents an interferogram. Colorbar is related to average spatial coherence of interferogram represented by the line connecting the two dots (i.e SAR images)

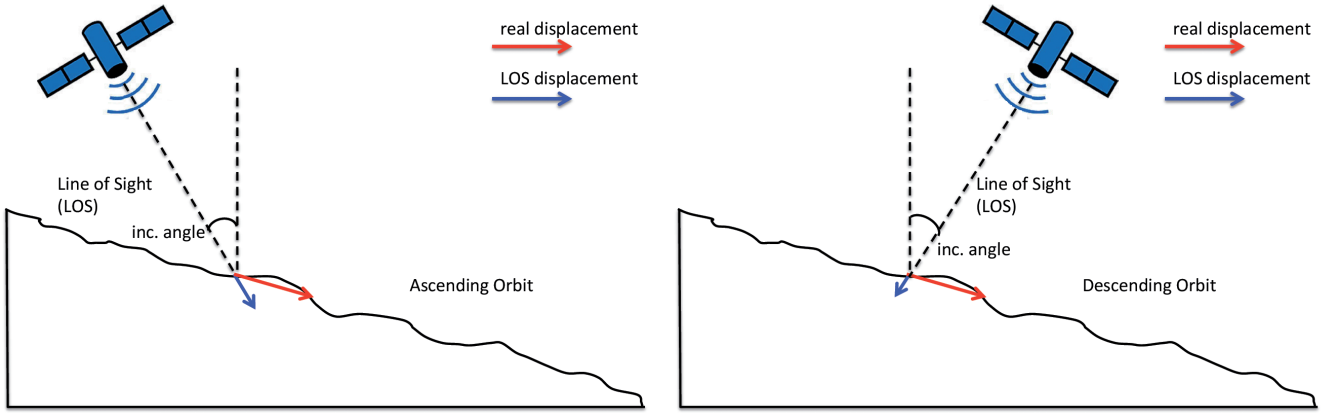

Fig. 5 - Difference between ascending (left) and descending (right) orbits to observe displacements over the studied slope

analyses. To attain good information from such images, a DInSAR-based approach was adopted, starting from single interferograms. Considering a complete image connection graph (to generate high redundancy), 36 interferograms were created, coupling all images to each other. As can be observed in Fig. 6, using the L-band signal, very highly coherent interferograms have been obtained, even with the high temporal and normal baselines, compared with those in Fig. 4. Furthermore, the topographic phase has been subtracted (using an available 20 m resolution DEM), thus providing 36 Differential Interferograms that allowed for the observation of the displacement phase contributions.

Because no A-DInSAR analysis was feasible and the area was relatively small, we performed a manual analysis of the best interferograms. The first step to attain reliable results regarding displacement occurrences was the detection and subtraction of the residual topographic component on differential interferograms. In this case, the residual heights have been estimated using a multi-image approach, more specifically, the Quasi-Persistent Scatterers (QPS) method (Perissin & Wang, 2012). Using the QPS approach, a sub-selection of points characterised by a very high and stable backscattering signal has been selected, thus estimating the phase related to the residual heights, exploiting all generated interferograms and weighing such pixels on the basis of their spatial coherence value. Local height information, derived from InSAR data, has been used to refine the original DEM to remove this re-estimated topographic component from the newly generated interferograms.

Starting from this redundant dataset, a quality threshold based on a spatial coherence value (>0.5) has been applied, thereby selecting the 24 best interferograms to perform the displacement investigation. In Tab. 5, the interferograms used for the further investigation stages are listed. Clearly, despite the selection performed to keep only the best interferograms, no images have been discarded, and all of them have been used to provide the highest possible temporal coverage.

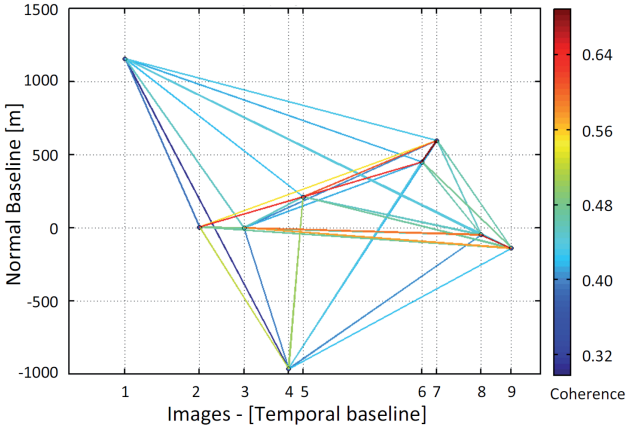

Fig. 6 - Graphs showing image connections related to ALOS PALSAR data-stack. Each dot represents an image in accordance with numeration of Tab. 3.3. Images are plotted in time (X axis) and space, represented by normal baseline (Y axis).). Each line represents an interferogram. Colorbar is related to average spatial coherence of interferogram represented by the line connecting the two dots (i.e SAR images)

INTERFEROMETRIC RESULTS

The 24 differential interferograms shown in Tab. 5 have been analysed to investigate the interferometric signals to detect and quantify any possible displacements.

We removed the topography as finely as possible using the QPS approach. However, a small residual topographic component may persist. To distinguish and separate that component from the displacement component, a criterion based on a double check was applied:

i) The phase signal related to the topography is proportional to B_n; thus, if a given interferometric feature varies proportionally with B_n, it is reasonable to assume that it is due to residual topography;

ii) Once a given interferometric signal is hypothesised to be in relation with the displacement, it is possible to observe the

persistence of the signal using the redundant interferograms because the signal should be temporally congruent with the interferogram data-set, generated by crossing all images. This also aided in understanding the time interval when the displacement processes occurred.

The examination of such interferograms allowed for the detection of some interferometric features (identified as "anomalies") recursively present in some of them. Such anomalies, whose presence along the interferometric set was apparently random, have been properly interpreted by applying the principles described above. In this way, it was possible to detect three small areas of the investigated slope that were characterised by interferometric features that can be interpreted as displacements that occurred within the examined period. By ordering the interferograms temporally (with the master images sorted in temporally ascending order) and also considering the B_n values, it was possible to identify the interferometric features related to the displacements by discarding those related to the topographic residual phase; moreover, it was possible to define the time interval when the detected displacements occurred.

The three small areas are localized in Fig. 7, and they are related to portions of the geocoded wrapped interferograms shown in Fig. 8, Fig. 9 and Fig. 10. Once a given interferometric feature was identified (red boxes inside the figures), it was "tracked" on all of the interferograms, marking those where it appeared. The first analysis of the detected phase signals was to distinguish the residual topographic features from the displacements. To attain this objective, as explained above, we checked the presence/absence of such anomalies in relation to the B_n values. As you can see, the presence of these anomalies is not directly linked to B_n; interferograms 1, 2, 8, 22 and 23 in Fig. 8, Fig. 9 and Fig. 10 are characterised by large baseline values, but they do not show the presence of such anomalies. In contrast, the detected phase signals are present in the other interferograms independently of B_n; for example, for all areas, interferograms 10 and 15 are characterised by the above-mentioned anomalies, even with small values of B_n.

This approach allowed for the definition of these phase signals due to displacements. Red borders surrounding some figures in Fig. 8, Fig. 9 and Fig. 10 identify interferograms with phase signals caused by displacements.

To confirm this deduction, selected interferograms have also been interpreted from a temporal point of view. In this perspective, redundant use of SAR images allowed the observation of the temporal congruency of the interferometric signals. Because the data used for this analysis are simple wrapped differential interferograms, atmospheric artefacts, decorrelation effects and general noise could still be present. For this reason, the use of the same image for several interferograms reduces the risk of losing information, which could be masked by such disturbances affecting any single image. Furthermore, as explained in section 4, the use of the same SAR image in more than one interferogram has also been crucial in defining with reliable accuracy the time interval when the detected processes occurred.

ID	Master-Slave	Temporal baseline [days]	Normal baseline [m]
1	20061223-20070810	230	1151
2	20061223-20071226	368	1155
3	20061223-20090630	920	706
4	20061223-20090815	966	560
5	20061223-20091231	1104	1205
6	20061223-20100402	1196	1295
7	20070810-20071226	138	3
8	20070810-20080512	276	970
9	20070810-20080627	322	206
10	20070810-20091231	874	53
11	20070810-20100402	966	143
12	20071226-20080627	184	209
13	20071226-20090630	552	449
14	20071226-20090815	598	595
15	20071226-20091231	736	50
16	20071226-20100402	828	140
17	20080512-20091231	598	916
18	20080627-20090630	368	240
19	20080627-20091231	552	259
20	20080627-20100402	644	349
21	20090630-20090815	46	146
22	20090630-20100402	276	589
23	20090815-20100402	230	735
24	20091231-20100402	92	89

Tab. 5 - ALOS PALSAR interferograms used for the investigation of past displacements

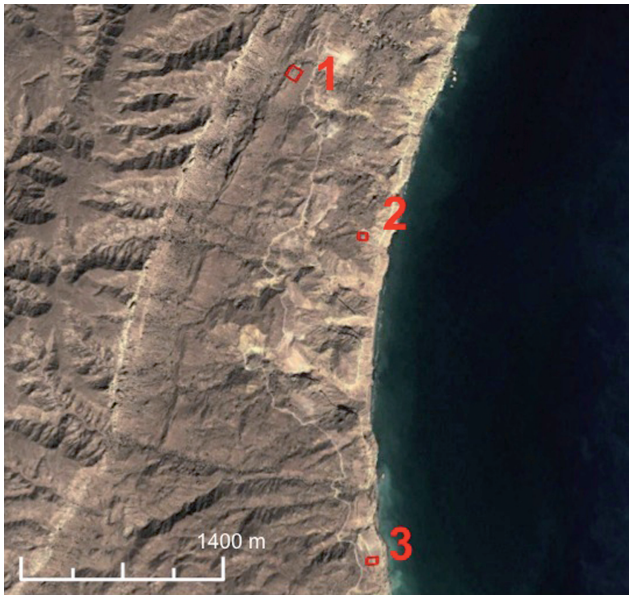

Fig. 7 - Localization of three small areas affected by instability processes detected by ALOS PALSAR interferograms (imagery from Google Earth V. 7.1.2.2041, DigitalGlobe, 2014)

In Tab. 6, all interferograms used for phase signal analysis and interpretation are reported as crosses between available images. Dark grey cells indicate an interferogram discarded because of the coherence below the threshold value; light grey cells indicate a null interferogram (i.e., master and slave images are the same); green cells indicate the absence of a phase signal related to a displacement; and red cells represent a displacement detected in the three areas where interferometric anomalies have been recognised. This graphic representation also helps to temporally define the instability phenomena, which occurred in a well-identified time interval between June 27th 2008 and June 30th 2009.

None of the generated interferograms computed by pairing images acquired before June 27th, 2008 show any anomalies that may be related to displacements. The same results is obtained for images acquired after that date. However, by pairing images acquired before and after this date, we obtained interferograms

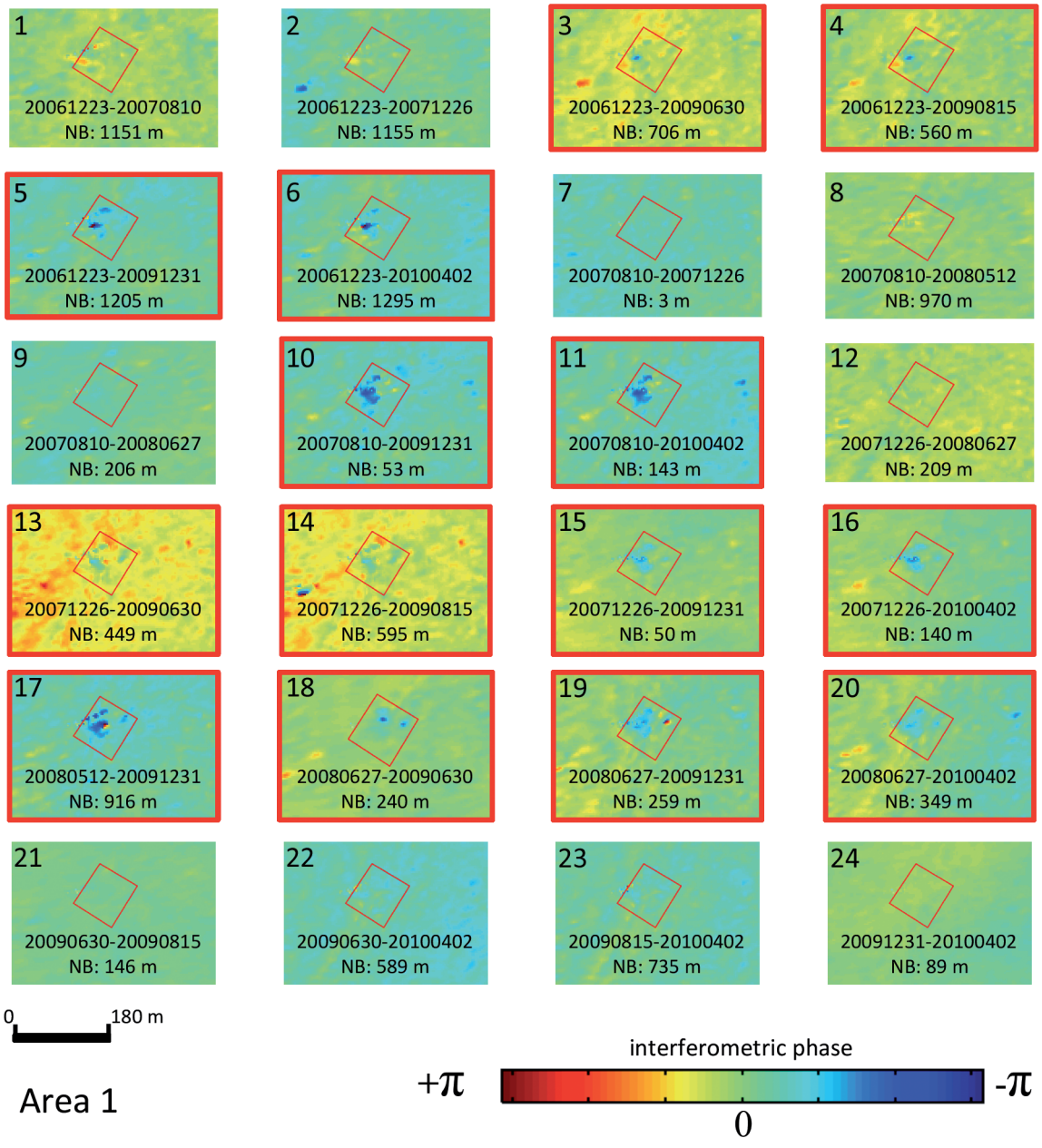

Fig. 8 - Interferometric anomaly detected in the area 1 (inside red boxes). The red bounds indicate the presence of anomaly, interpreted as displacements, in the given interferogram

characterised by the presence of observable displacements in the phase signal. These results are confirmed by all of the interferograms computed by using all possible combinations. Therefore, in the time interval between June 2008 and June 2009, some instability processes occurred in the three identified areas.

Considering the results shown in Fig. 8, Fig. 9 and Fig. 10, the phase signals can be considered to quantitatively estimate detected displacements starting from the angular values of the wrapped phase. Because the PALSAR sensor operates with a 236 mm wavelength (Tab. 4), the maximum detectable phase difference (equal to 2π and represented by the transition from red to blue colour in the interferograms) corresponds to a displacement equal to $\lambda/2$ (118 mm) along the LOS. Using the very high coherence attained, these weak, small and localised indications of movements were clear enough to be quantitatively estimated. The interferometric phase difference between the anomalies and the surrounding pixels has been consid-

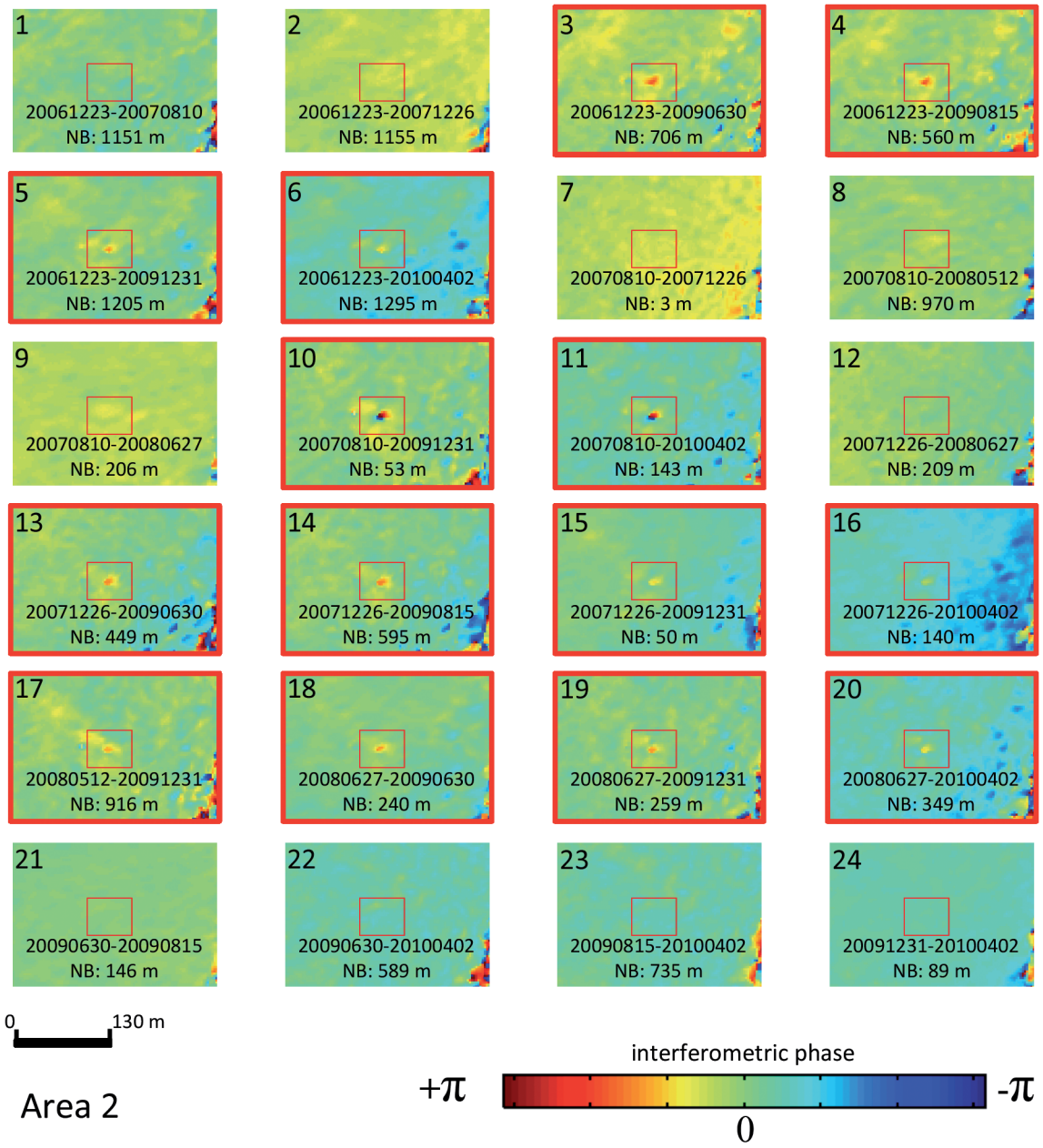

Fig. 9 - Interferometric anomaly detected in the area 2 (inside red boxes). The red bounds indicate the presence of anomaly, interpreted as displacements, in the given interferogram

ered. Area 1 (Fig. 8), in the northern part of the study area, is approximately 90x70 m, located near the tectonic line coincident with the coastal rock cliff. Considering all of the analysed interferograms, a 40-45 mm LOS displacement away from the satellite was detected. Area 2 (Fig. 9), smaller than the previous area, is very localised (approximately 40x40 m), showing slightly smaller displacements (approximately 30 mm along the LOS). In this case, the displacements are in the direction away from the satellite. Area 3 (approximately 50x50 m) is very near the coast and is located on a portion of the slope involved in the landslide that occurred in the period August 2011-June 2012. Because of the small dimensions of the area affected by displacements in the period under investigation and because the detected displacements are very small (approximately 35 mm along the LOS in the direction away from the satellite), it is not possible to directly relate the previously observed displacements with the wider instability process that affected the slope in 2011-2012.

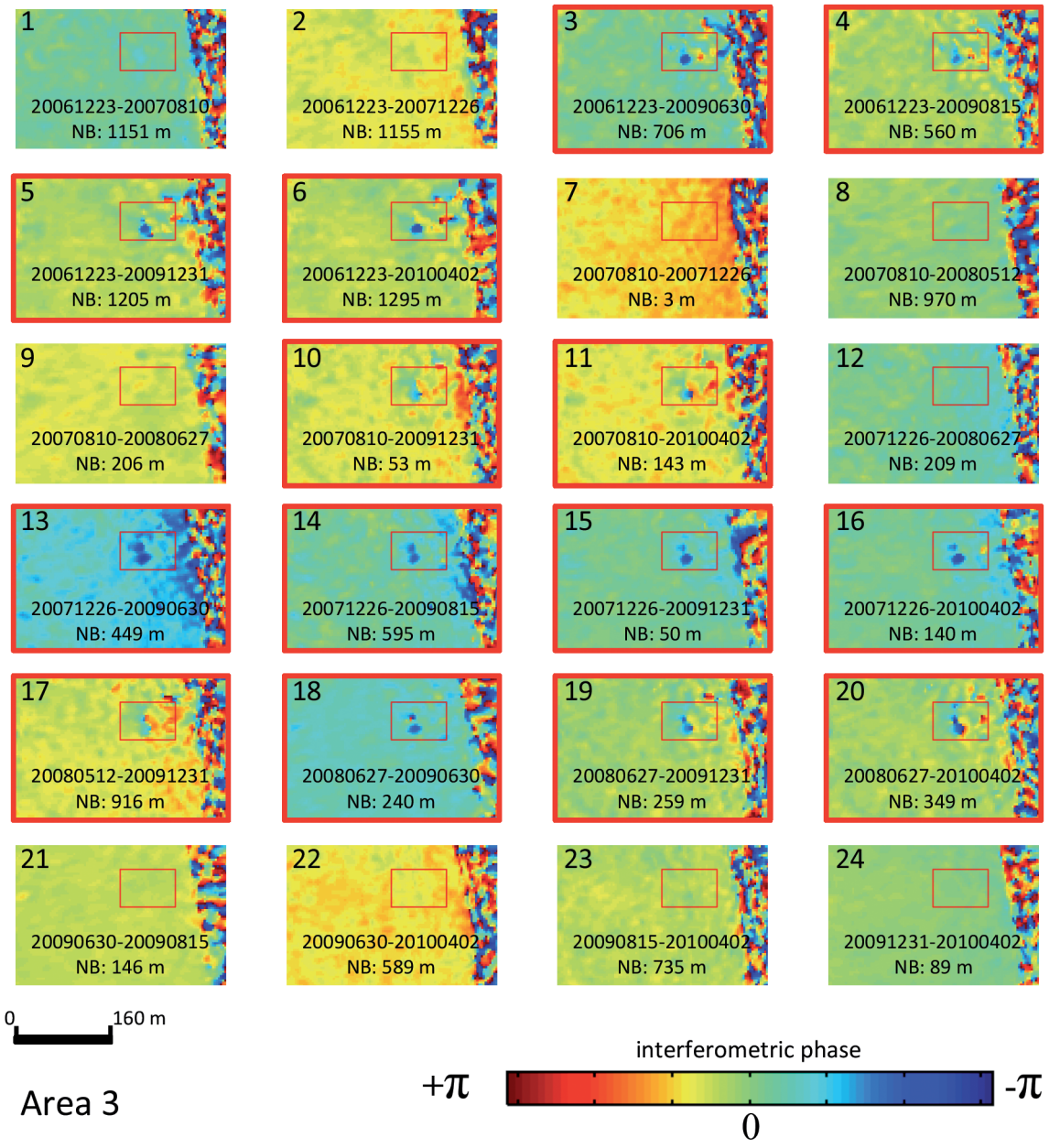

Fig. 10 - Interferometric anomaly detected in the area 3 (inside red boxes). The red bounds indicate the presence of anomaly, interpreted as displacements, in the given interferogram. The belt with casual coloured pattern on the right is due to the sea surface, which is characterized by null coherence

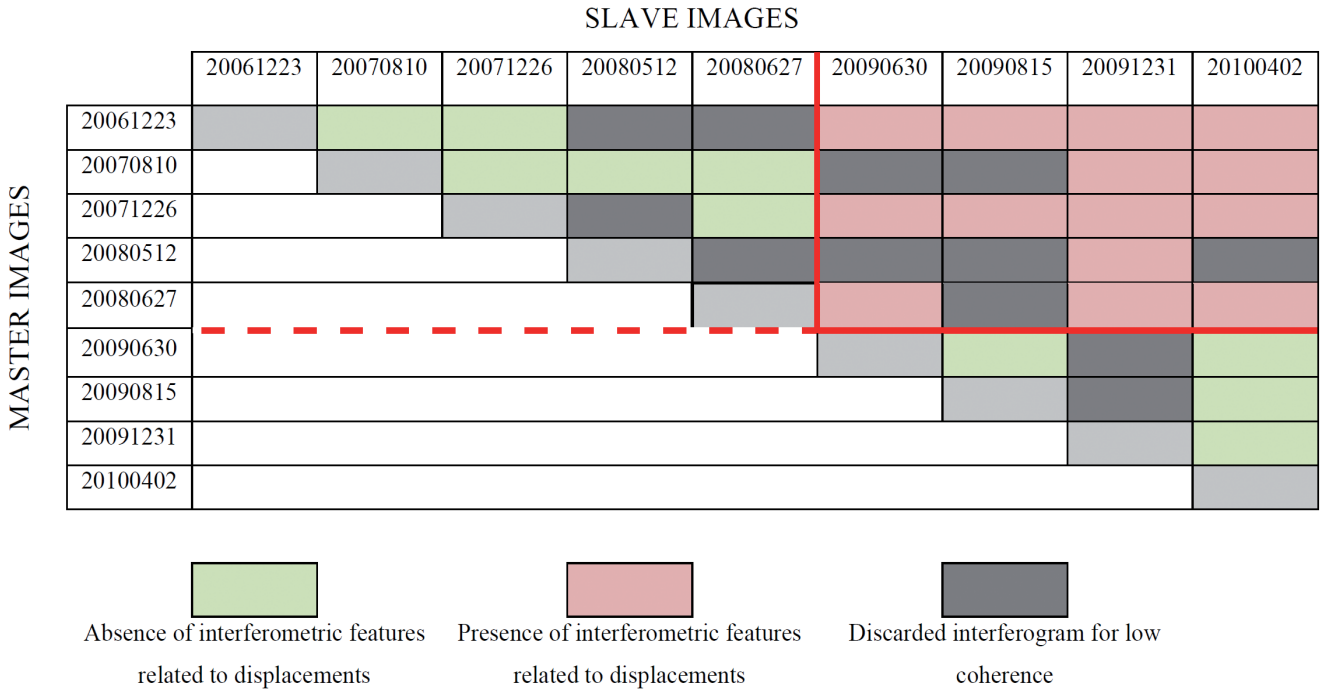

Tab. 6 - Temporal distribution of detected interferometric anomalies along interferograms time series. Green boxes identify absence of anomalies; red boxes identify presence of anomalies; dark grey boxes identify discarded interferograms in accordance with Tab. 3.5. Light grey boxes identify null interferograms because of coincidence between master and slave images

DISCUSSION

The methodology used to investigate past displacements for the present case study is based on a classical approach of SAR interferometry, which is the direct examination of computed interferograms. Many automated algorithms to extract information from SAR data-stacks exist; however, they are likely not capable of achieving the results herein shown. A-DInSAR methods could not provide trustable and reliable results by using such poor data-stacks, especially in the very difficult conditions of this case, with very small displacements circumscribed in restricted areas, the presence of non-linear displacements, low temporal image frequency, and the absence of further supporting information. Detailed work manually analysing phase signal contributions through a slope-oriented approach allowed us to extract more information than expected from the available data.

We began by distinguishing the topographic components from the displacement phase contributions manually. It could be argued that the height estimation (to refine the DEM used to compute the differential interferograms) was partially performed using automated methods, but that was not the case for the displacement estimation. This is because also with the few available images, the estimation of heights remains a linear problem dependent on the normal baseline and thus more easily accomplished. In contrast, the estimation of displacements is much more controlled by the number of images.

The low temporal resolution of the available dataset did not allow better definition of the temporal development of the detected phenomena; thus, we have to accept a 1-year approximation for such events. Furthermore, we do not know if the detected displacements developed as single, impulsive events, or if they are the result of slow processes that developed over a longer period (several weeks or months). At the timescale of the adopted dataset, the detected displacements can be considered "impulsive" because they were not distributed throughout the entire period of the images. In addition, for this reason, such phenomena would most likely not be detected by an automated A-DInSAR analysis, even with a larger dataset.

The use of the L-band data, acquired by the ALOS PALSAR satellite, also played a key role in the attainment of the results. In addition to the advantages in terms of the high coherence discussed in section 1.3.3, the use of these data has the additional advantage of being less dependent on phase ambiguity due to high, rapid displacements. In such circumstances, with displacements that occurred in a time interval not covered by many images, or with rapid, impulsive movements, the risk of losing information due to wavelength limits was very high. Other data, such as C-band (wavelength: ~56 mm) or even X-band (wavelength: ~30 mm) data, which are more affected by phase ambiguity problems, would most likely not be able to provide such information with $\lambda/2$ values equal to ~28 mm and ~15 mm, respectively.

CONCLUSIONS

The evolution of instability processes affecting a coastal slope in the Sultanate of Oman has been defined by using satellite SAR interferometry. Thanks to archive data provided by the Japanese ALOS PALSAR satellite, an investigation based on the combination of DInSAR and QPS techniques allowed us to achieve quantitative results about surface displacements occurred within the time-span covered by the SAR images (December 2006-April 2010).

The approach used in this work allowed us to overcome the limitation caused by the limited number of images in the area, which was not sufficient to perform A-DInSAR analyses. The QPS method has been used to obtain a more accurate DEM to better discriminate the displacement phase signal from the topographic information.

A manual interpretation of the generated interferograms has been carried out to properly observe the occurred displacements. The application of an automated algorithm, in fact, could easily disguise them because they were not continuous in space and time. More specifically, the used approach was carried out by analysing temporal (i.e. acquisition dates of the images) and geometrical (i.e. normal baseline) parameters characterising all interferograms that were computed with the highest possible redundancy. The phase signals related to displacement detected in the interferograms have been analysed in terms of their relation with the normal baseline and the congruency with their temporal distribution along the whole dataset.

The slope instability processes have been defined in time (occurrence between June 2008-June 2009), and the related displacements have been quantitatively estimated. The proposed approach demonstrates the capability to derive information about past displacements by satellite SAR images also in case when advanced interferometric techniques are not feasible due to the limited number of images in the dataset. Therefore, it can be considered a useful investigative solution also in remote and not urbanized areas where a limited knowledge on geomorphological and geological settings is available and where monitoring data about past evolution of displacement phenomena do not exist. It can also provide an early prior indication that can be deepened during in-situ investigations related to major construction on large areas.

ACKNOWLEDGMENTS

The present work has been carried out thanks to the European Space Agency in the frame of the Cat-1 project “Landslides forecasting analysis by time series displacement derived from Satellite and Terrestrial InSAR data” (Id 9099) and Rocksoil S.p.A., which provided basic geological data.

REFERENCES

Barrett E.C. (2013) - *Introduction to environmental remote sensing*. Routledge.

Béchennec F., Le Métour J., Platel J.P. & Roger J. (1993) - *Geological map of the Sultanate of Oman, scale 1:1,000,000*. Oman Ministry of Petroleum and Minerals, Directorate General of Minerals.

Berardino P., Fornaro G., Lanari R. & Sansosti E. (2002) - *A new algorithm for surface deformation monitoring based on small baseline differeential SAR interferograms.* IEEE Trans. Geosci. Remote Sensing. **40**: 2375-2383.

Bozzano F. & Rocca A. (2012) - *Remote monitoring of deformation using satellite SAR interferometry.* Geotechnical News, **30**(2): 26.

Carnec C., Massonnet D. & King C. (1996) - *Two examples of the use of SAR interferometry on displacement fields of small spatial extent.* Geophysical Research Letters, **23**(24): 3579-3582.

Chen F., Lin H., Li Z., Chen Q. & Zhou J. (2012) - *Interaction between permafrost and infrastructure along the Qinghai-Tibet Railway detected via jointly analysis of C-and L-band small baseline SAR interferometry.* Remote Sensing of Environment, **123**: 532-540.

Chen F., Lin H. & Hu X. (2014) - *Slope superficial displacement monitoring by small baseline SAR interferometry using data from L-band ALOS PALSAR and X-band TerraSAR: a case study of Hong Kong, China.* Remote Sensing, **6**(2): 1564-1586. doi:10.3390/rs6021564

Ferretti A., Prati C. &. Rocca F. (2001) - *Permanent scatterers in SAR interferometry*. IEEE Trans. Geosc. and Remote Sens., **39**(1): 8-20.

Ferretti A., Fumagalli A., Novali F., Prati C., Rocca F. & Rucci A. (2011) - *A new algorithm for processing interferometric data-stacks: SqueeSAR.* Geoscience and Remote Sensing, IEEE Transactions on, **49**(9): 3460-3470.

Fournier M., Bellahsen N., Fabbri O. & Gunnell Y. (2004) - *Oblique rifting and segmentation of the NE Gulf of Aden passive margin*. Geochemistry, Geophysics, Geosystems, **5**(11).

Fruneau B., Achache J. & Delacourt C. (1996) - *Observation and modelling of the Saint-Étienne-de-Tinèe landslide using SAR interferometry.* Tectonophysics, **265**: 181-190.

Gabriel A.K. & Goldstein R.M. (1988) - *Crossed orbit interferometry: theory and experimental results from SIR-B.* Int.J. Remote Sensing, **9**(5): 857-872.

García-Davalillo J. C., Herrera G., Notti D., Strozzi T. & Álvarez-Fernández I. (2014) - *DInSAR analysis of ALOS PALSAR images for the assessment of very slow landslides: the Tena Valley case study*. Landslides, **11**: 225-246. doi:10.1007/s10346-012-0379-8.

Ghezzi G., Peralta J.C., Bianchi A., Sartini S., Anfuso A., Creatini F., Cassitelli M., Ghezzi R., Pellegrini M., Porsia D. & Rizza L. (2012) - *Geophysical site investigation for Hasik landslides stretch from km 7+000 to km 8+500* (Unpublished technical report).

Goldstein R., Zebker H.A. & Werner C.L. (1988) - *Satellite radar interferometry: two-dimensional phase unwrapping,* Radio Science, **23**(4):713-720.

Goldstein R., Engelhardt H., Kamb B. & Frolich R. (1993) - *Satellite radar interferometry for monitoring ice-sheet motion: application to an Antarctic ice stream*. Science, **262**: 1525-1530.

Hanssen R. (2001) - *Radar interferometry, data interpretation and error analysis*. Kluwer Academic Publishers.

Hooper A., Zebker H., Segall P. & Kampes B. (2004) - *A new method for measuring deformation on volcanoes and other natural terrains using InSAR persistent scatterers.* Geophysical Research Letters, **31**(23): L23611. doi:10.1029/2004GL021737

Jebur M.N., Pradhan B. & Tehrany M.S. (2013) - *Using ALOS PALSAR derived high-resolution DInSAR to detect slow-moving landslides in tropical forest: Cameron Highlands, Malaysia.* Geomatics, Natural Hazards and Risk (ahead of print): 1-19. doi:10.1080/19475705.2013.860407.

Kampes B.M. (2006) - *Radar interferometry persistent scatterers technique*. (Springer Ed.) - Dordrecht, The Netherlands.

Kwok R. & Fahnestock M.A. (1996) - *Ice sheet motion and topography from radar interferometry.* IEEE Transactions on Geoscience and Remote Sensing, **34**(1): 189-200. doi:10.1109/36.481903.

Lanari R., Lundgren P., Manzo M. & Casu F. (2004) - *Satellite radar interferometry time series analysis of surface deformation for Los Angeles, California.* Geophysical Research Letters, **31**(23).

Lauknes T.R. (2004) - *Long-term surface deformation mapping using small-baseline differential SAR interferograms.* Unpublished Master Thesis, Department of Physics and Technology, University of Tromsø.

Lepvrier C., Fournier M., Bérard T. & Roger J. (2002) - *Cenozoic extension in coastal Dhofar (southern Oman): implications on the oblique rifting of the Gulf of Aden.* Tectonophysics, **357**(1): 279-293.

Li F. & Goldstein R. (1987) - *Studies of multi-baseline spaceborne interferometric synthetic aperture radar*. In: International Geoscience and Remote Sensing Symposium, Ann Arbor, 18-21 May 1987: 1545-1550.

Li F.K. & Goldstein R.M. (1990) - *Studies of multibaseline spaceborne interferometric synthetic aperture radars*. IEEE Transactions on Geoscience and Remote Sensing, **28**(l): 88-97.

Massonnet D., Rossi M., Carmona C., Adragna F., Peltzer G., Feigl K. & Rabaute T. (1993) - *The displacement field of the Landers earthquake mapped by radar interferometry*. Nature, **364**(6433): 138-142.

Massonnet D., Feigl K., Rossi M. & Adragna F. (1994) - *Radar interferometric mapping of deformation in the year after the Landers earthquake*. Nature, **369**(6477): 227-230.

Massonnet D., Briole P., & Arnaud A. (1995) - *Deflation of Mount Etna monitored by spaceborne radar interferometry.* Nature, **375**(6532): 567-570.

Mercolli I., Briner A.P., Frei R., Schönberg R., Nägler T.F., Kramers J. & Peters T. (2006) - *Lithostratigraphy and geochronology of the Neoproterozoic crystalline basement of Salalah, Dhofar, Sultanate of Oman.* Precambrian Research, **145**: 182-206.

Perissin D. (2008) - *Validation of the submetric accuracy of vertical positioning of PSs in C-band.* Geoscience and Remote Sensing Letters, IEEE, **5**(3): 502-506.

Perissin D. (2009) - *SARPROZ Manual* http://ihome.cuhk.edu.hk/~b122066/index_files/download.htm.

Perissin D., Wang Z. & Wang T. (2011) - *The SARPROZ InSAR tool for urban subsidence/manmade structure stability monitoring in China*. Proc. of ISRSE 2010, Sidney, Australia, 10-15 April 2011.

Perissin D. & Wang T. (2012) - *Repeat-Pass SAR Interferometry with partially coherent targets*. IEEE Trans. on Geosc. and Remote Sens. **50**(1): 271, 280.

Perissin D., Wang Z. & Lin H. (2012) - *Shanghai subway tunnels and highways monitoring through Cosmo-SkyMed Persistent Scatterers.* ISPRS Journal of Photogrammetry and Remote Sensing, **73**: 58-67.

Platel J.P. & Roger J. (1989) - *Evolution geodynamique du Dhofar (Sultanat d'Oman) pendant le Crétacé et le Tertiaire en relation avec l'ouverture du golfe d'Aden*. Bull. Soc. Geol. Fr., **2**: 253-263.

Platel J.P., Roger J., Peters T.J., Mercolli I., Kramers J.D. & Le Me´tour J. (1992) - *Geological map of Salalah, Sultanate of Oman; sheet NE 40-09, scale 1:250000,* Oman Ministry of Petroleum and Minerals, Directorate General of Minerals.

Prati C., Rocca F., Monti Guarnieri A. & Damonti E. (1990) - *Seismic Migrataion For SAR Focussing: Interferometrical Applications.* IEEE Transactions on Geoscience and Remote Sensing, **28**(4): 627-640.

Riedel B. & Walther A. (2008) - *InSAR processing for the recognition of landslides*. Advances in Geosciences, **14**(14): 189-194.

Robertson A.H.F. & Bamkhalif K.A.S. (2001) - *Late Oligocene-early Miocene rifting of the northeastern Gulf of Aden: basin evolution in Dhofar (southern Oman)*. In Ziegler P.A., Cavazza W., Robertson A.H.F. & S. Crasquin-Soleau S. (Eds) - *Peri-Tethys Memoir 6: Perihal- 00021620, version Tethyan Rift/Wrench Basins and Passive Margins*. Mém. Mus. Natn. Hist. Nat., **186**: 641-670.

Roger J., Platel J.P., Cavelier C. & Bourdillon de Grissac C. (1989) - *Donntes nouvelles sur la stratigraphie et l'histoiregtologique du Dhofar (Sultanat d'Oman)*. Bull. Sot. GCol. Fr. **8**(2): 265-277.

Roger J., Platel J.P., Berthiaux A. & Le Me ´Tour J. (1992) - *Geological map of Hawf with Explanatory Notes; sheet NE 39-16, scale 1:250000*, Oman Ministry of Petroleum and Minerals, Directorate General of Minerals.

Simons M., Fialko Y. & Rivera L. (2002) - *Coseismic deformation from the 1999 Mw 7.1 Hector Mine, California, earthquake as inferred from InSAR and*

GPS observations. Bulletin of the Seismological Society of America, **92**(4): 1390-1402.

Singh L.P., Westen C.J., Champati Ray P.K. & Pasquali P. (2005) - *Accuracy assessment of InSAR derived input maps for landslide susceptibility analysis: a case study from the Swiss Alps*. Landslides, **2**(3): 221-228. doi:10.1007/s10346-005-0059-z

Singhroy V., Mattar K. & Gray A. (1998) - *Landslide characterisation in Canada using interferometric SAR and combined SAR and TM images*. Advances in Space Research, **21**(3).

Stramondo S., Bozzano F., Marra F., Wegmuller U., Cinti F.R., Moro M. & Saroli M. (2008) - *Subsidence induced by urbanisation in the city of Rome detected by advanced InSAR technique and geotechnical investigations.* Remote Sensing of Environment, **112**(6): 3160-3172.

Strozzi T., Farina P., Corsini A., Ambrosi C., Thüring M., Zilger J., Wiesmann A., Wegmuller U. & Werner C. (2005) - S*urvey and monitoring of landslide displacements by means of L-band satellite SAR interferometry*. Landslides, **2**(3): 193-201. doi:10.1007/s10346-005-0003-201

Strozzi T., Delaloye R., Kääb A., Ambrosi C., Perruchoud E. & Wegmüller U. (2010) - *Combined observations of rock mass movements using satellite SAR interferometry, differential GPS, airborne digital photogrammetry, and airborne photography interpretation*. Journal of Geophysical Research: Earth Surface, **115**(F1): 2003-2012.

Tong X., Sandwell D.T. & Fialko Y. (2010) - *Coseismic slip model of the 2008 Wenchuan earthquake derived from joint inversion of interferometric synthetic aperture radar, GPS, and field data*. Journal of Geophysical Research: Solid Earth, **115**(B4): 1978-2012.

Van Leijen F. J. & Hanssen R.F. (2007) - *Persistent scatterer density improvement using adaptive deformation models.* In Geoscience and Remote Sensing Symposium, 2007. IGARSS 2007. IEEE International: 2102-2105. IEEE.

Watchorn F., Nichols G.J. & Bosence D.W.J. (1998) - *Rift-related sedimentation and stratigraphy, southern Yemen (Gulf of Aden).* In: Purser B.H., Bosence D.W.J. (Eds.) - *Sedimentation and Tectonics of Rift Basins: Red Sea- Gulf of Aden.* Chapman & Hall, London: 165-191.

Wei M. & Sandwell D.T. (2010) - *Decorrelation of L-band and C-band interferometry over vegetated areas in California.* Geoscience and Remote Sensing, IEEE Transactions on, **48**(7): 2942-2952.

Received February 2014 - Accepted May 2014